Fiber Breakage and Dispersion in Carbon-Fiber-Reinforced Nylon 6/Clay Nanocomposites

Hu Zhou, Zhongzhong Qian, Xiangfu Meng, Yanfen Ding, Shimin Zhang, Mingshu Yang

Key Laboratory of Engineering Plastics, Beijing National Laboratory for Molecular Sciences (BNLMS), Chinese Academy of Sciences, Institute of Chemistry, Beijing 100080, China

Received 15 December 2006; accepted 15 May 2007
DOI 10.1002/app.26818
Published online 17 July 2007 in Wiley InterScience (www.interscience.wiley.com).

ABSTRACT: In this paper, short carbon-fiber-reinforced nylon 6/clay nanocomposites are prepared via melt compounding, and fiber breakage and dispersion during processing are studied. The influences of clay and processing conditions on fiber breakage and dispersion are taken into consideration. It is found that the presence of organoclay can improve fiber dispersion, which is due to dispersion at the nanoscale of exfoliated clay sheets with large aspect ratio. The bimodal distribution of fiber length is observed in fiber-reinforced nanocomposites, which is similar to that in conventional fiber-reinforced composites. The improvement of fiber breakage at moderate organoclay loadings is also observed, which is ascribed to the rheological and lubricating effects induced by organoclay. © 2007 Wiley Periodicals, Inc. J Appl Polym Sci 106: 1751–1756, 2007

Key words: fiber breakage; fiber dispersion; carbon fiber; clay; nanocomposites

INTRODUCTION

Polymer/clay nanocomposites containing clay platelets with thickness of 1 nm and diameter from 10^1 to 10^3 nm, typically nylon 6 (polyamide 6, PA6)/montmorillonite (MMT) nanocomposites, have received widespread attention in scientific and industrial fields because they reveal superior mechanical and barrier properties at very low loading levels (<5 wt %).[1–3] However, compared to conventional fiber-reinforced polymer composites (FRPC), the two-component PA6/MMT nanocomposites are still insufficient in the mechanical properties and therefore their usage is limited in some special applications.[4,5] To make the most of their superior properties, it is necessary and convenient to further reinforce the PA6/MMT nanocomposites with conventional fibers, such as fiberglass and carbon fibers.

In structure, nanocomposites and conventional microcomposites are distinct in the filler dimensions; for example, the thickness of filler particles which in reality are individual clay platelets in a fully exfoliated polymer/clay nanocomposite is about 10^4 times smaller than the fiber diameter in FRPC. Therefore, the two composites can be combined in a new type of three-component hybrid composite, which can lead to significant improvement in their mechanical and other properties. Some works have demonstrated that nanocomposites as the matrix can further improve the properties of conventional FRPC.[6–9] Especially, short fiber-reinforced polymer nanocomposites (SFRPNC) can achieve desired improvement of the mechanical properties at lower fiber loading levels than conventional short fiber-reinforced polymer composites (SFRPC).

It is well known that, to make the most of reinforcement, the aspect ratio of the fibers must be kept sufficiently large in the SFRPC. However, fiber breakage is severe during conventional extrusion and injection molding in the manufacturing/processing of SFRPC.[5,10] Hence, elucidating, controlling, and improving fiber breakage are crucial for SFRPC.

Fiber breakage during manufacturing/processing two-component SFRPC has been widely studied. It has been observed that under extrusion and injection conditions most of the damage occurred in the screw-melting zone.[11,12] Gupta et al.[12] considered the fiber breakage as a two-stage phenomenon: first, fibers bent and broke at the solid–melt interface following an attrition mechanism; second, the broken pieces flowed with the polymer melt and experienced further breakage due to postbuckling deformation. The theory of fiber breakage in a shear flow was developed by Forgacs and Mason[13] and Salinas and Pittman.[14] They found that the viscosity of systems and the shear rate were critical of fiber breakage in a shear flow. Hence, the efficient means of improving fiber breakage are to decrease the viscosity and the shear rate by varying processing conditions and machine designs. Grillo et al.[15] and

Correspondence to: M. Yang (yms@iccas.ac.cn).
Contract grant sponsor: Major Basic Research Projects of China; contract grant number: 003CB615600.

Journal of Applied Polymer Science, Vol. 106, 1751–1756 (2007)

Ramani et al.[16] found that varying screw and die design was the most efficient way of controlling fiber breakage during manufacturing/processing SFRPC. However, because it was not convenient to modify the design of screw and die during manufacturing/processing SFRPC, varying processing conditions became preferred for improving the fiber breakage. But until now, an efficient control of fiber breakage is still not very satisfying during manufacturing/processing SFRPC.

FRPNC are similar to conventional FRPC in the structure if polymer nanocomposite is taken as a homogeneous matrix. However, the rheological properties of these systems are very different due to the presence of nanoparticles, which has been observed by some researches.[17,18] Obviously, the rheological effect induced by nanoparticles has some influences on manufacturing/processing SFRPNC, especially, fiber breakage and dispersion, but it is still unknown.[6–9] Furthermore, dispersed clay perhaps induces some other effects which could influence the fiber breakage and dispersion, but these effects are also unclear. So in this study, the fiber breakage and dispersion are investigated for short carbon-fiber-reinforced nylon 6/clay nanocomposites, and the influences of clay and processing conditions on fiber breakage and dispersion were taken into consideration respectively.

EXPERIMENTAL

Materials

Nylon 6 (Type 2, with density 1.13 g/cm^3) was supplied by Shanghai Plastic Products (China). Sodium montmorillonite (Na-MMT), with a cation-exchange capacity of 85 meq/100 g and a density of 2.83 g/cm^3, was purchased from Zhangjiakou Qinghe Chemical Plant (China). Octadecyl diethanolamine was supplied by Shanghai Jinshan Chemical (China). Synthesized fluoromica (MICA, with mean diameter 40 μm) was supplied by Sinoma Advanced Materials (China). Chopped carbon fiber (CF, Panex®33, with diameter 7.2 μm, length 0.85 cm, density 1.81 g/cm^3, tensile strength 3800 MPa and tensile modulus 228 GPa) was purchased from Zoltek Companies (USA). Epoxy resin (Type 0144) was purchased from Wuxi Resin Factory of Blue Star New Chemical Materials (China). Other reagents were of commercial products and used as-received. Organic montmorillonite (OMMT) was prepared by the cation-exchange reaction with octadecyl diethanolamine salt formed by protonizing the amine.

The as-received carbon fiber was first oxidized under air at 440°C for 30 min. Then, the oxidized carbon fibers were immersed into epoxy–acetone solution where epoxy resin was added at 5 wt % of carbon fibers to be treated. Subsequently, this slurry was left at room temperature for 24 h for the removal of solvent and fibers were dried in an oven under vacuum at 60°C for 3 h.

Sample preparation

PA6, OMMT, Na-MMT, and MICA were dried under vacuum at 85°C for 24 h before use. The composites were prepared by blending the components at 240°C in a HAAKE Rheomix-600 internal mixer (Germany) with a volume of 69 mL and a couple of Sigma-shape counter-rotating blades. The internal mixer was operated at a rotary speed of 45 rpm. The sequential feeding processing method was adopted in all experiments: PA6 without and with OMMT was first melted in the mixer for 2 min, then the epoxy-treated CF were added within 30 s and finally mixed for 3 min or otherwise specified. For comparison, Na-MMT and MICA were also used instead of OMMT and processed in the same manner. The composites are denoted by the notation of the components followed by the weight ratio of the components themselves. For example, PA6/10|CF/1 and PA6/50|OMMT/1 are codes for two-component composites; PA6/50|CF/5|OMMT/3 stands for a three-component composite containing 50 weight parts PA6, 5 parts CF, and 3 parts OMMT.

The bar-shape specimens with a dimension of 45 × 5.8 × 3.1 mm^3 were prepared by injection molding at 255°C using a Mini-Max molder (CSI-183MMX, Custom Scientific Instruments).

Observation of fiber dispersion/aggregation

A selective dissolution method (Molau test) was applied to evaluate fiber dispersion state in the composites. Two-tenth gram of each sample was placed in an ampoule flask and about 5 mL of formic acid (90 wt %) was added to dissolve the PA6 matrix. After PA6 matrix was solved completely, the yielded suspension was homogenized by light shaking and then photographed immediately using a digital camera to obtain the image of fiber dispersion/aggregation in formic acid. To ensure the accuracy of the observation, five or more samples were adopted for the same composition.

For observation of fiber dispersion/aggregation in solid state, the bar test specimens were sliced with a thickness of 20 μm along the direction of injection molding using a Leica RM2155 microtome. The slices were placed on glass slides and observed using a Leica DM LP-MP30 microscope.

Figure 1 Optical photographs of Molau tests of the composites in formic acid. From left to right: PA6/20|CF/1|OMMT/1, PA6/20|CF/1|OMMT/0.4, PA6/20|CF/1, and PA6/20|CF/1. The treated CF is mixed for 10 min for the rightmost sample or 3 min for the others.

Determination of FLD

To distinguish every single fiber, the suspensions from Molau test were diluted with formic acid till the fiber concentration reached about 0.2 wt % in the suspension. Then, several droplets were taken out rapidly and were placed on microscope glass slides after the suspension from Molau test was homogenized by light shaking. Next, these slides were dried in an oven, and observed using a Leica DM LP-MP30 microscope. About 30 images were obtained for each sample, and were digitalized through a CCD camera connected to a computer. Measuring all fibers ($\sim$ 800) in these photos provided a representative value of the average fiber length and the histogram of percentage of fiber against fiber length range. To ensure the accuracy of the measurement, five samples were adopted for the same composition. It was verified that the fiber length distribution (FLD) results were repeatable with only very small deviations for different samples of the same composition.

Characterization of clay dispersion

XRD patterns are obtained using a Rigaku D/max 2400 diffractometer (40 kV, 200 mA; Cu Kα, λ = 0.154 nm; reflection mode). XRD scans are performed on the composite specimens, as well as on Na-MMT and OMMT powder, at ambient temperature with a 2θ range between 1° and 10°, at a scanning rate of 4°/min and a scanning step of 0.02°.

Clay dispersion in the composites is investigated by a Hitachi H-800 transmission electron microscope apparatus at an acceleration voltage of 200 kV. Ultrathin sections are obtained by cryogenic ultramicrotoming the bar-shaped specimens along the injection direction.

RESULTS AND DISCUSSION

Fiber dispersion

The fiber dispersion in composites is evaluated by both Molau test and direct observing the solid slices. In formic acid, the PA6 matrix is dissolved while the black CF fillers are suspended after shaking, as shown in Figure 1. For the two-component PA6/CF composites, precipitation of CF takes place immediately and few agglomerates of fiber bundles are observed in the suspensions (which are quite clear), even though the mixing time of melt compounding lasted for 10 min (the rightmost sample in Fig. 1). For the three-component PA6/CF/OMMT composites, the suspensions are much darker and seem more homogeneous, especially fiber bundles disappear when the organoclay content reaches 5 wt % of PA6 (PA6/20|CF/1|OMMT/1). The optical microscopy images of the solid slices in Figure 2 also reveal

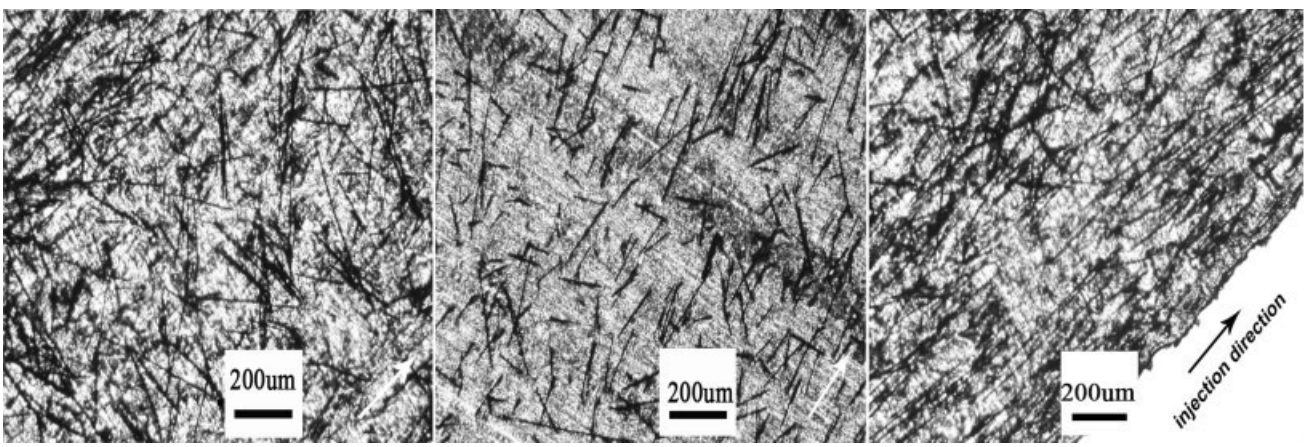

Figure 2 Optical micrographs of the solid slices of the composites. Left: PA6/20|CF/1; Middle: PA6/20|CF/1|OMMT/1; Right: PA6/20|CF/1|Na-MMT/1. The injection direction is indicated by the arrow.

Figure 3 Optical photographs of Molau tests of the composites in formic acid. From left to right: PA6/20|CF/1|OMMT/1, PA6/20|CF/1|Na-MMT/1, PA6/20|CF/1|MICA/1, and PA6/20|CF/1.

a nonuniform dispersion of CF in the PA6/CF composite and a quite uniform dispersion of CF in the PA6/CF/OMMT composite. Although increasing the mixing time can reduce fiber bundles in PA6/CF composites, this does not achieve the dispersion as of PA6/CF/OMMT composite; indeed, the fiber length will be diminished. Hence, the improvement in fiber dispersion induced by the organoclay is of great importance for SFRPNC.

To gain insight into the effect of the organoclay, Na-MMT- or MICA-filled PA6/CF composites are also investigated. As shown in Figure 3, black agglomerations are present in the suspensions of PA6/CF/Na-MMT and PA6/CF/MICA composites but absent in the suspensions of PA6/CF/OMMT composite. The optical microscopy image of the solid slices in Figure 2 also reveals a nonuniform dispersion of CF in the PA6/CF/Na-MMT composite. The microscopic analysis (including optical microscopy, transmission electron microscopy, and XRD, seen in Figs. 4 and 5) of the composites show that MICA is dispersed in micrometric scale as its original size, Na-MMT is intercalated as stacks of large size, and only OMMT is almost fully exfoliated to individual silicate platelets. The above results indicate that the improvement in fiber dispersion is correlated to the exfoliated clay platelets at nanometric scale. We believe that it is the rotation of exfoliated clay platelets of large aspect ratio (about 50–100 in our experiments) that promotes fiber dispersion. It will be discussed later in detail.

Fiber length and distribution

Table I shows the number mean fiber lengths $(\bar{L} = \sum n_i l_i / \sum n_i)$ for composites with different organoclay loadings. The addition of organoclay increases $\bar{L}$ in PA6/20|CF/1|OMMT/1 and PA6/20|CF/1|OMMT/1.6 composites but decreases $\bar{L}$ in other composites. This indicates that the fiber breakage depends on the organoclay content. In fact, this dependency is also observed in the above experiments on fiber dispersion, as shown in Figure 1. Obviously, the optimal organoclay content is determined by equilibrium of the rheological and lubricating effects induced by organoclay. It will be discussed later in detail.

A bimodal FLD is observed in the composites, as seen for examples in Figure 6 (other samples show similar bimodal length distribution). Analog bimodal distribution was observed previously by Gupta et al.[12] in the processing of long fiberglass-reinforced

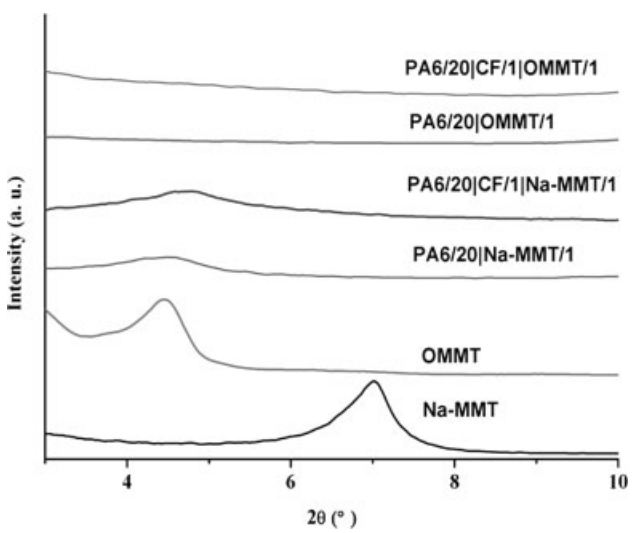

Figure 4 XRD patterns of Na-MMT, OMMT, and nylon 6 composites.

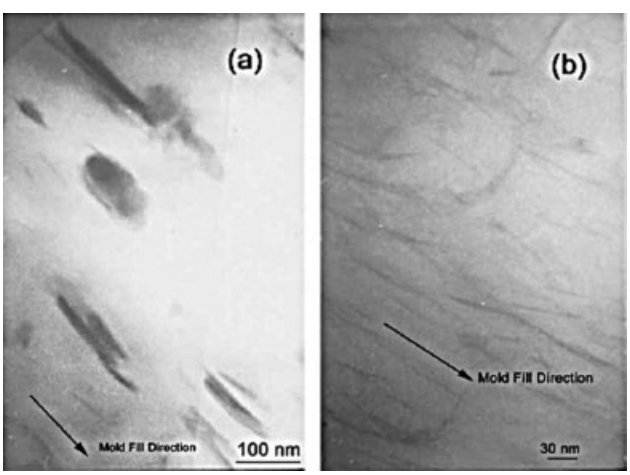

Figure 5 TEM images of nylon 6 composites taken close to the surface region: (a) PA6/20|Na-MMT/1 and (b) PA6/20|OMMT/1.

TABLE I
Effect of Organoclay Loadings on Fiber Length in Composites[a]

Composite	Melt torque (Nm)	$L/D < 10$		$L/D \geq 10$		
		vol %	$\bar{L}_{-10}$(μm)	vol %	$\bar{L}_{+10}$(μm)	$\bar{L}$(μm)
PA6/20|CF/1	4.8	4.22	55.0	95.78	261	226
PA6/20|CF/1|OMMT/0.4	4.2	5.20	54.3	94.80	254	213
PA6/20|CF/1|OMMT/0.6	4.2	5.10	55.2	94.90	248	211
PA6/20|CF/1|OMMT/1	3.7	4.16	55.1	95.84	292	248
PA6/20|CF/1|OMMT/1.6	3.4	5.24	55.2	94.76	286	235
PA6/20|CF/1|OMMT/2	3.2	5.86	54.2	94.14	255	210

[a] The melt torque was recorded by the end of mixing.

composites. Obviously, the presence of organoclay does not change the two-stage phenomenon of fiber breakage during processing. During the processing of PA6/CF/OMMT composites, the first-stage fiber breakage occurs at the solid–melt interface after fibers are added. In this stage, the fiber breakage is not influenced by organoclay, confirmed by the small variation of the volume contents of long ($L/D \geq 10$, L/D: aspect ratio) and short ($L/D < 10$) fibers in different composites, as shown in Table I. After that, fibers flow with the suspension and the second-stage fiber breakage occurs. In this stage, organoclay has a complex influence on fiber breakage, as seen in Table I for the variation of the number mean length of long ($L/D \geq 10$) fibers in different composites.

Table II shows the number mean fiber lengths for composites with different CF loadings. In the PA6/CF and PA6/CF/OMMT composites, $\bar{L}$ decrease with increasing the CF loading. This is caused by the increase in viscosity, as shown in Table II, and the increase in attrition between fibers. The investigation of Gibson[19] on packing effects in convergent flow revealed that increasing the fiber volume fraction would increase the fiber-to-fiber attrition, leading to an increasing fiber breakage, especially when $V_f^{\max}$ was reached. In Table II, it is also found that the addition of organoclay results in longer fibers, especially, the increase of fiber length is more noticeable when the fiber volume fraction is far less than the theoretical maximum fiber volume fraction ($V_f^{\max}$).

We believe that in the presence of organoclay, the increase in fiber length is mainly due to the decrease in viscosity and the lubrication action of the nanometric clay platelets located around the CF fibers. The decrease of the viscosities, a main rheological effect induced by organoclay, which has been well characterized in the past (for examples on PA6/clay nanocomposites see Fornes et al.[20] and Zhang et al.[21]), is revealed by the decrease of the melt torques of composites, as shown in Tables I and II. This decrease can improve fiber breakage according to the theory of fiber breakage under the shear flow.[13,14] On the other hand, the lubrication action of the nanometric clay platelets not only reduces fiber breakage, but also improves fiber dispersion.

The nanometric clay platelets can efficiently infiltrate into fiber bundles in the melt for their small sizes, and moreover, will rotate in the shear flow.[13,14] The perturbation induced by the rotation of the nanometric clay platelets will appear inside fiber bundles, which can promote fiber dispersion. Furthermore, only when the volume fraction of

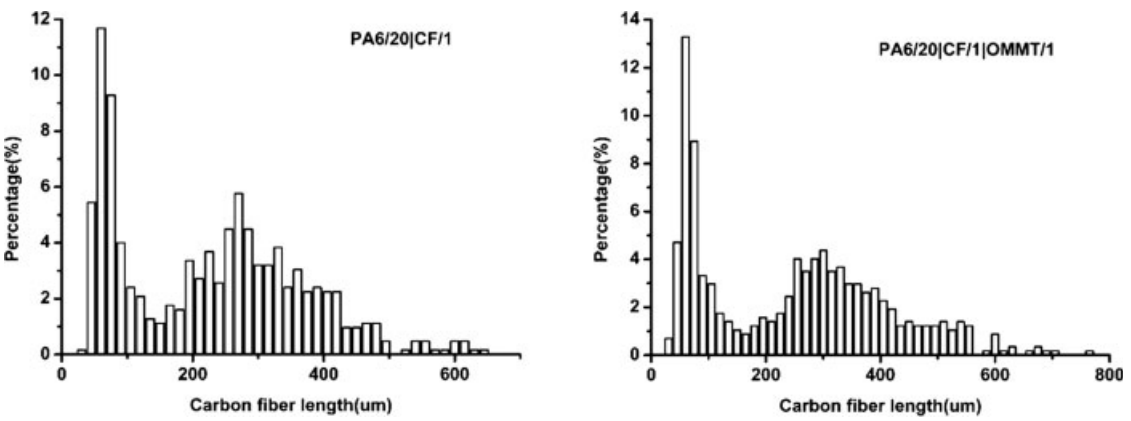

Figure 6 Length distribution of carbon fiber in the composites with different organoclay loadings.

TABLE II
Effect of CF Loadings on Fiber Length in Composites[a]

Composite	$\bar{L}$(μm)	Melt torque (Nm)	V_f^{max} (%)[b]	V_f (%)[c]
PA6/20|CF/0.2	261	4.0	2.76	0.623
PA6/20|CF/1	226	4.8	3.19	3.05
PA6/20|CF/2	206	5.0	3.50	5.91
PA6/20|CF/0.2|OMMT/1	349	2.5	2.06	0.611
PA6/20|CF/1|OMMT/1	248	3.7	2.90	2.99
PA6/20|CF/2|OMMT/1	224	4.5	3.21	5.80

[a] The melt torque was recorded by the end of mixing.
[b] $V_f^{max} \cong D/L$.[19]
[c] $V_f \cong (m_f/\rho_f)/(m_n/\rho_n + m_f/\rho_f + m_c/\rho_c)$, where m and ρ stand for weight ratio and density, respectively. Subscripts f, n, and c denote fiber, PA6, and clay, respectively.

organoclay is high enough, the fibers can be dispersed completely because the perturbation can spread all over the melt in this instance. However, microparticles cannot improve fiber dispersion because they cannot efficiently infiltrate into fiber bundles for their large sizes, as in the cases of PA6/CF/MMT and PA6/CF/MICA composites.

As discussed above, the nanometric clay platelets locate around the fiber bundles and rotate in the shear flow. This also results in decreasing the fiber-to-fiber interactions and increasing the ability of fiber motion, which means that the nanometric clay platelets produce a lubrication action, and hence diminishes fiber breakage. However, when the content of clay is too high, fiber breakage will increase, as observed in our experiments. In high clay loading polymer nanocomposites, organoclay is not exfoliated completely, and cannot efficiently infiltrate into fiber bundles. As a result, the lubrication action weakens.

CONCLUSIONS

In this paper, fiber breakage and dispersion have been investigated in short carbon-fiber-reinforced nylon 6/clay nanocomposites. It is found that the addition of organoclay diminishes fiber breakage and improves fiber dispersion when the content of organoclay reaches 5 wt % of PA6, whereas the inorganic clay and MICA cannot improve fiber dispersion. The experiments indicate that the improvement of fiber dispersion is correlated to the exfoliated clay sheets at nanometric scale.

The bimodal distribution of fiber length is observed in all experiments. This indicates that the presence of organoclay does not change the two-stage phenomenon of fiber breakage during processing: the first-stage fiber breakage occurring at the solid–melt interface, which is not influenced by organoclay, and the second-stage fiber breakage occurring in a shear flow, which is influenced by organoclay. The observed improvement of fiber breakage at moderate organoclay loadings is ascribed to the rheological and lubricating effects induced by organoclay.

The experiments and the results are well explained: the improvement of fiber dispersion comes from the rotation of exfoliated clay sheets with large aspect ratio, and the improvement of fiber breakage comes from the decrease of viscosity caused by organoclay and lubrication action of the nanometric clay platelets.

References

1. Usuki, A.; Kojima, Y.; Kawasumi, M.; Okada, A.; Fukushima, Y.; Kurauchi, T.; Kamigaito, O. J Mater Res 1993, 8, 1179.
2. Liu, L.; Qi, Z.; Zhu, X. J Appl Polym Sci 1999, 71, 1133.
3. Shah, R. K.; Paul, D. R. Polymer 2004, 45, 2991.
4. Drozda, T. J., Ed. Composite Applications. Society of Manufacture Engineers: Dearborn, Michigan, 1989.
5. Schwartz, M. M., Ed. Composite Materials Handbook; McGraw-Hill: New York, 1992.
6. Akkapeddi, M. K. Polym Compos 2000, 21, 576.
7. Wu, S. H.; Wang, F. Y.; Ma, C. C. M.; Chang, W. C.; Kuo, C. T.; Kuan, H. C.; Chen, W. J Mater Lett 2001, 49, 327.
8. Vlasveld, D. P. N.; Bersee, H. E. N.; Picken, S. J Polymer 2005, 46, 10269.
9. Hassan, A.; Hornsby, P. R.; Folkes, M. J Polym Test 2003, 22, 185.
10. Kelly, A.; Tyson, W R J Mech Phys Solids 1965, 13, 329.
11. Turkovich, R. V.; Erwin, L. Polym Eng Sci 1983, 23, 743.
12. Gupta, V. B.; Mittal, R. K.; Sharma, P. K.; Mennig, G.; Wolters, J. Polym Compos 1989, 10, 8.
13. Forgacs, O. L.; Mason, S. G. J Colloid Sci 1959, 14, 457.
14. Salinas, A.; Pittman, J. F. T. Polym Eng Sci 1981, 21, 23.
15. Grillo, J.; Andersen, P.; Papazoglou, E. J Reinforc Plast Compos 1993, 12, 311.
16. Ramani, K.; Bank, D.; Kraemer, N. Polym Compos 1995, 16, 258.
17. Drubetski, M.; Siegmann, A.; Narkis, M. Polym Compos 2005, 26, 454.
18. Konishi, Y.; Cakmak, M. Polymer 2005, 46, 4811.
19. Gibson, A. G. Plast Rubb Process Appl 1985, 5, 95.
20. Fornes, T. D.; Yoon, P. J.; Paul, D. R. Polymer 2003, 44, 7545.
21. Zhang, B.; Ding, Y.; Chen, P.; Liu, C.; Zhang, J.; He, J.; Hu, G. Polymer 2005, 46, 5385.